Int. J. Electrochem. Sci., 8 **(2013)** 6807 - 6817

International Journal of
ELECTROCHEMICAL
SCIENCE
www.electrochemsci.org

Electrochemical Properties of Hollow, Spherical Li_2O-SnO_2-Cu-C Nanocomposite Powders Prepared by Spray Pyrolysis

Yong Seung Jang, Jung Hyun Kim, Jung-Kul Lee[*]*, Yun Chan Kang*[*]

Department of Chemical Engineering, Konkuk University, 1 Hwayang-dong, Gwangjin-gu, Seoul 143-701, Korea
[*]E-mail: yckang@konkuk.ac.kr, jkrhee@konkuk.ac.kr

Received: 11 March 2013 / *Accepted:* 29 March 2013 / *Published:* 1 May 2013

Hollow and spherical Li_2O-SnO_2-Cu-C nanocomposite powder is prepared by spray pyrolysis. Examination of the nanocomposite powder shows that Li_2O-SnO_2-Cu particles are uniformly distributed over a hollow C matrix. Li_2O-SnO_2-Cu-C nanocomposite powder has better cycling performance than do Li_2O-SnO_2-CuO-C and Li_2O-SnO_2-Cu_2O-C nanocomposite powders. The uniform mixing of electrochemically inactive Cu metal and electrochemically active SnO_2 improves the cycling performance of Li_2O-SnO_2-Cu-C powder. The charge capacity of Li_2O-SnO_2-Cu-C nanocomposite powder drops from 547 to 449 mAh g^{-1} after 130 cycles at a current density of 700 mA g^{-1}; the corresponding capacity retention is 82%. The capacity retention of the Li_2O-SnO_2-CuO-C and Li_2O-SnO_2-Cu_2O-C nanocomposite powders after 130 cycles is 44% and 52%, respectively. The cycling performance of the SnO_2-Cu-C and Li_2O-SnO_2-CuO nanocomposite powders is compared to that of Li_2O-SnO_2-Cu-C powder. The presence of Li_2O and a C matrix improve the rate performance as well as the cycling performance of the nanocomposite powders by minimizing the crystal growth of SnO_2 during repeated charging and discharging cycles.

Keywords: composite powders; anode material; spray pyrolysis; lithium-ion battery

1. INTRODUCTION

SnO_2-based transition metal oxides with various compositions and exhibiting high reversible capacities have been developed as anode materials for lithium-ion batteries [1-17]. Inactive or active components were mixed using various techniques to form SnO_2-MO_x (M = Cu, Co, Si, Ru) composite powders with diverse structures to overcome the limitations of pure SnO_2 anode materials. However, the initial capacity loss and cycle retention of the composite powders must be further improved for use in high-performance lithium-ion batteries.

Recent research has introduced composites of Li_2O and transition metal oxides with three-dimensional networks formed by electrostatic spray deposition (ESD) [16-19]. These composites when formed on metal meshes of Ni or stainless steel showed a high reversible capacity, good capacity retention, and a significant improvement in rate capability [16-19]. Furthermore, the addition of Li_2O suppressed the aggregation and mechanical deterioration of Li–metal alloy during cycling and also decreased the irreversible capacity loss that accompanies the use of SnO_2 negative electrodes [16-19]. In previous reports, the electrochemical properties of the composite thin films of Li_2O and transition metal oxides formed by ESD have been studied [16-19]. However, in commercial lithium-ion batteries, powders composed of micron-sized spherical particles are commonly used as anode materials. C-coated material is widely applied to improve the electrochemical properties of transition metal oxides because the addition of C increases the conductivity of the powders and minimizes the growth of active components during cycling [13-15, 20-24].

In this study, hollow and spherical Li_2O-SnO_2-Cu-C nanocomposite powder was prepared by spray pyrolysis. The electrochemical properties of the Li_2O-SnO_2-Cu-C nanocomposite powder were compared to those of Li_2O-SnO_2-CuO-C, Li_2O-SnO_2-Cu_2O-C, Li_2O-SnO_2-CuO, SnO_2-Cu-C, and Cu_6Sn_5-Cu_3Sn-C nanocomposite powders. Furthermore, the effects of Li_2O, Cu metal, and the C matrix on the electrochemical properties of the composite powders were clarified.

2. EXPERIMENTAL

Li_2O-SnO_2-CuO-C composite powder was prepared directly by the spray pyrolysis of a solution containing Li, Sn, Cu, and C components. The spray pyrolysis system consisted of a droplet generator, quartz reactor, and powder collector. A 1.7-MHz ultrasonic spray generator with six vibrators was used to generate a large quantity of droplets, which were transported to a high-temperature tubular reactor using a N_2 carrier gas flowing at 10 L min^{-1}. The droplets evaporated, decomposed, and/or crystallized in the quartz reactor. The length and diameter of the quartz reactor were 1000 and 55 mm, respectively, and the temperature inside the reactor was fixed at 1000°C. The spray solution used for the pyrolysis was prepared by dissolving a stoichiometric ratio of $LiNO_3$ [Aldrich], $Cu(NO_3)_2 \cdot 3H_2O$ [Aldrich], and $SnCl_2 \cdot 2H_2O$ [Aldrich] in distilled water. The overall concentration of Li, Cu, and Sn components was 0.5 M. The concentration of sucrose, which was used as the C source, was 0.5 M. The powder prepared by spray pyrolysis underwent a post-treatment at temperatures between 400 and 600°C under a pure N_2 atmosphere to obtain the Li_2O-SnO_2-CuO(or Cu)-C composite powders.

The crystal structures of the composite powders were investigated using X-ray diffractometry (XRD, Rigaku DMAX-33) at the Korea Basic Science Institute (Daegu). The morphology of the composite powder particles was observed using scanning electron microscopy (SEM, JEOL JSM-6060) and transmission electron microscopy (TEM, JEOL, JEM-2010). The capacities and cycling properties of anodes made from the composite powders were measured using 2032-type coin cells. The anodes were prepared by mixing 28 mg of composite powder, 6 mg of carbon black, and 6 mg of sodium carboxymethyl cellulose (CMC) in distilled water. Li metal and polypropylene films were used

as the counter electrode and separator, respectively. The electrolyte was 1 M $LiPF_6$ mixed in a 1:1 volume ratio with ethylene carbonate/dimethyl carbonate (EC/DMC). The entire cell was assembled in a glove box under an argon atmosphere. The charge/discharge characteristics of the samples were measured at room temperature and under various current densities in the range 0.01–3.0 V.

3. RESULTS AND DISCUSSIONS

The morphology of Li_2O-SnO_2-CuO-C nanocomposite particles post-treated at 500°C under a N_2 atmosphere is shown in Fig. 1.

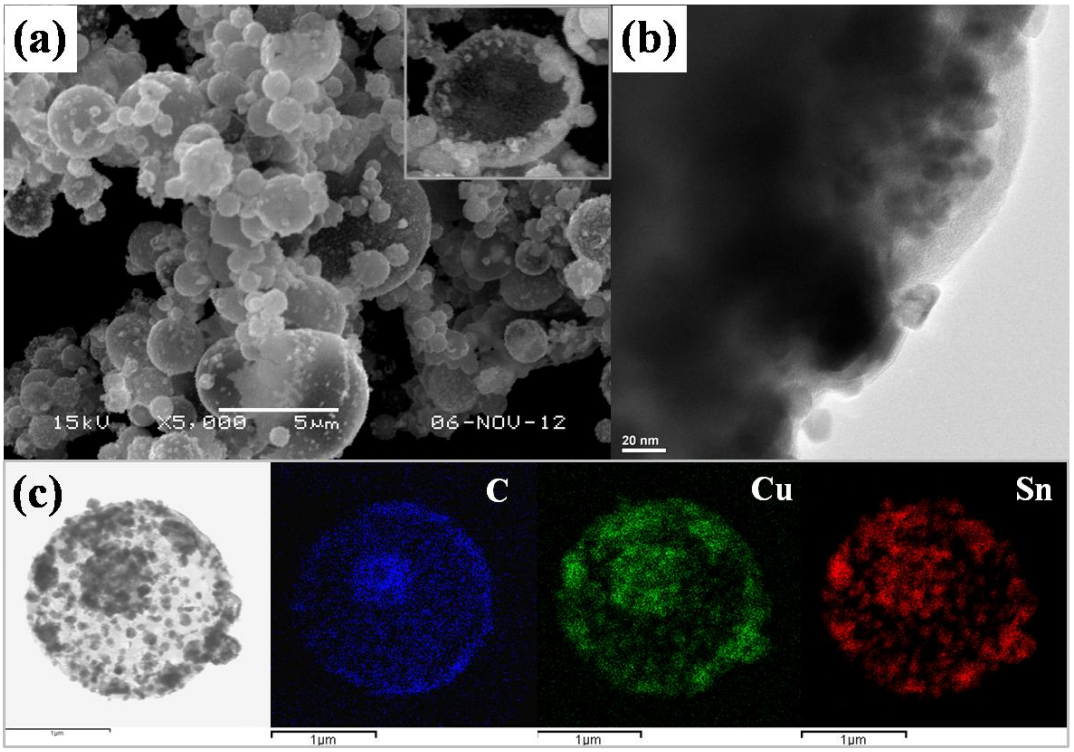

Figure 1. Morphology and dot-mapping images of Li_2O-SnO_2-CuO-C nanocomposite powder post-treated at 500°C.

The precursor powder particles prepared by spray pyrolysis had spherical shape and sizes in the micron range. The spherical shape of this precursor powder was maintained after the post-treatment at 500°C. The hollow structure of the nanocomposite powder was inferred from the SEM image as shown in Fig. 1 (a) of a broken particle. The TEM and dot-mapping images shown in Fig. 1 display the detailed structure of the Li_2O-SnO_2-CuO-C nanocomposite powder. Spherical nanoparticles several nanometers in diameter were uniformly distributed over the C matrix. The C matrix was formed by polymerization and carbonization in an inert gas atmosphere. In the dot-mapping images, all nanoparticles consisted of a uniform mixture of Sn and Cu components. Since the Li component could

not be detected in the EDS mapping images, the nanoparticles embedded in the C matrix were considered to be a uniform mixture of SnO_2, CuO, and Li_2O.

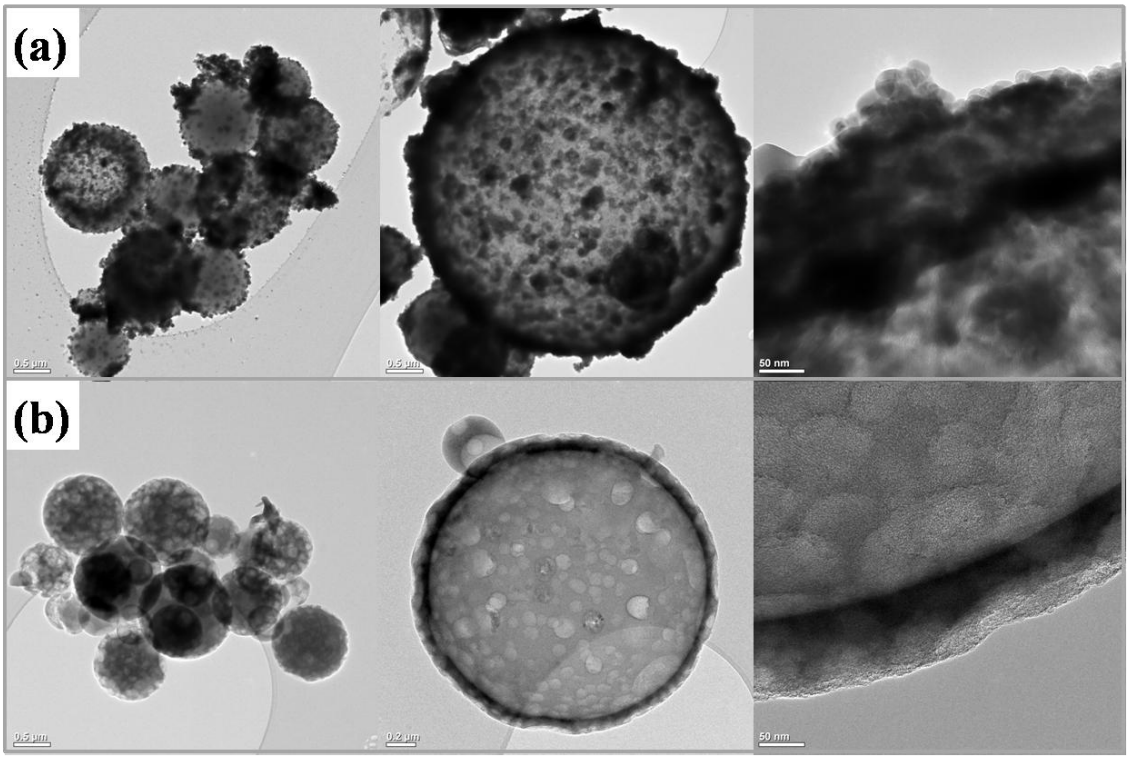

Figure 2. TEM images of the Li_2O-SnO_2-CuO-C nanocomposite powders post-treated at (a) 400 and (b) 600^{o}C.

Fig. 2 shows the morphologies of the nanocomposite powders treated at 400 and 600°C. The powder treated at 400°C had a similar morphology to that of the precursor powder, in which nanoparticles were dispersed in a spherical C matrix. On the other hand, the nanocomposite powder post-treated at 600°C had a spherical shape with a smooth surface. Nanoparticles containing Sn and Cu components were not detected in the TEM image as shown in Fig. 2b.

The relationship between the morphology change in the Li_2O-SnO_2-CuO-C nanocomposite powder and the post-treatment temperature was further clarified by examining the crystal structure of the powder as shown in Fig. 3. The precursor powders prepared directly by spray pyrolysis exhibited poor crystallinity because of the short residence time of the powder inside the quartz reactor (approximately 2 s). The presence of C matrix also inhibited the growth of the nanoparticles. The chief crystal structures observed in the precursor powder were attributed to SnO_2 and CuO. The peak intensity of the SnO_2 phase increased with increasing post-treatment temperatures up to 500°C. On the other hand, CuO reduced to Cu_2O and Cu at post-treatment temperatures of 450 and 500°C, respectively. Li_2O existed as a stable phase at post-treatment temperatures below 500°C. Therefore, it is concluded that the powders generated from post-treatment at 400, 450, and 500°C were Li_2O-SnO_2-CuO-C, Li_2O-SnO_2-Cu_2O-C, and Li_2O-SnO_2-Cu-C nanocomposites, respectively. Reduction of SnO_2

to Sn metal and the alloying reaction of Sn with Cu metal occurred at a high post-treatment temperature of 600°C.

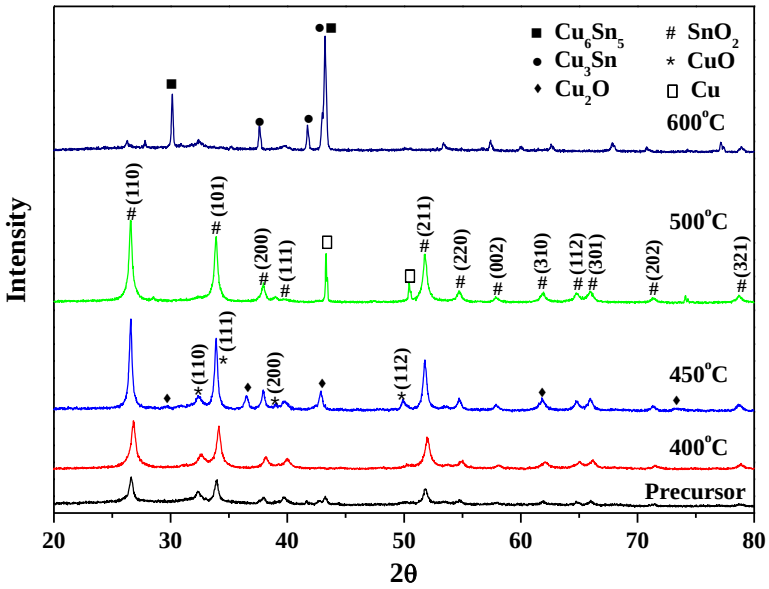

Figure 3. XRD patterns of the precursor and post-treated nanocomposite powders at various temperatures.

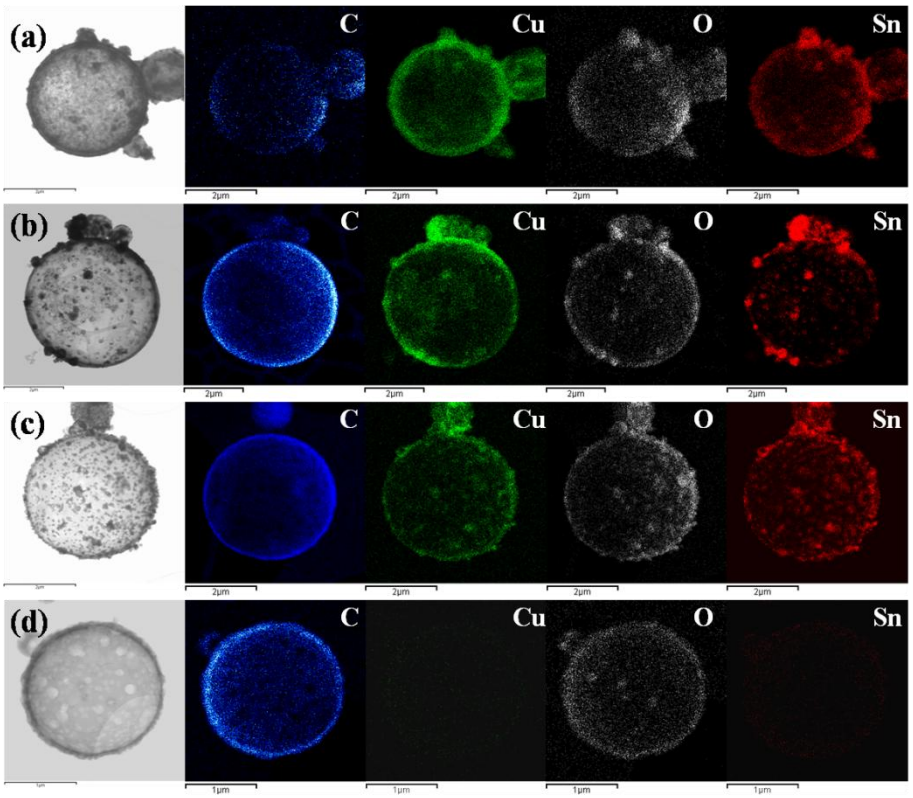

Figure 4. Dot-mapping images of Li_2O-SnO_2-CuO-C powders post-treated at (a) 400°C, (b) 450°C, (c) 500°C, and 600°C.

Thus, Cu_6Sn_5-Cu_3Sn-C nanocomposite powder was obtained at a post-treatment temperature of 600°C. Cu_6Sn_5 and Cu_3Sn alloys had low-melting points of 415 and 676°C, respectively. Therefore, melting of the Cu_6Sn_5 and Cu_3Sn alloys resulted in the phase separation of alloy powders and spherical C matrix during the post-treatment process. The dot-mapping images of the nanocomposite powder treated at 600°C as shown in Fig. 4 did not show Sn and Cu components in the spherical powder, but did reveal that the main components were C and O. The O component in the dot-mapping images originated from the Li_2O phase. Therefore, the hollow spherical particles shown in Fig. 2b are assumed to be C-Li_2O nanocomposites.

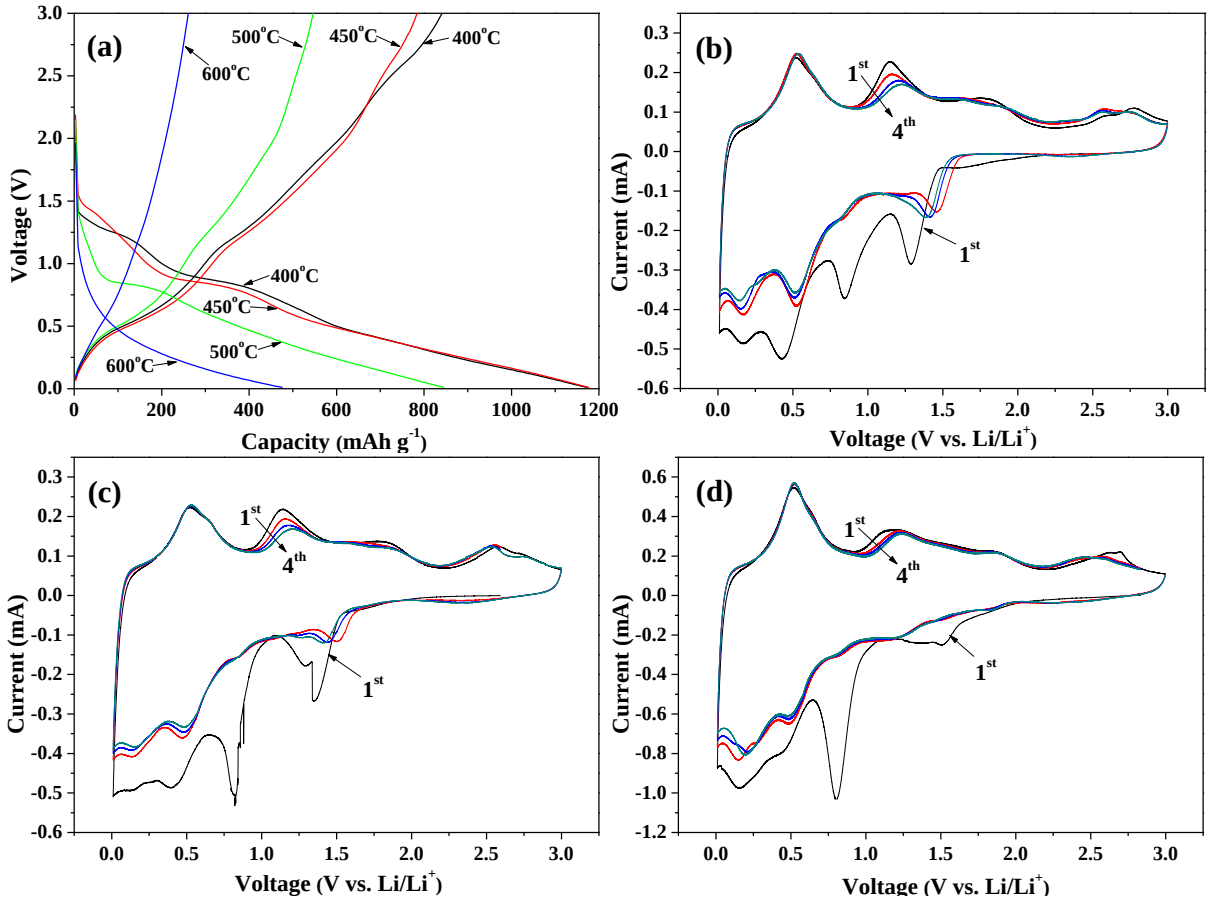

Figure 5. Initial charge/discharge curves and cycle voltammograms of the nanocomposite powders post-treated at various temperatures. (a) The initial cycle profile in the voltage range of 0.01-3 V at 700 mA g^{-1}. (b) (c) (d) Cycle voltammograms of the first four cycles at a scan rate of 0.01 mV s^{-1} in the voltage range of 0.01-3 V.

Fig. 5a shows the initial charge and discharge curves of the nanocomposite powders at a constant current density of 700 mA g^{-1} within the cutoff voltage range 0.01–3 V. The initial discharge curve of the Li_2O-SnO_2-CuO-C nanocomposite powder treated at 400°C had two plateaus near 1.3 and 0.8 V. These two voltage plateaus can be attributed to the reduction of SnO_2(IV) and CuO(II), respectively [25-27]. The Li_2O-SnO_2-Cu-C nanocomposite powder treated at 500°C had single plateau near 0.8 V, which is attributed to the reduction of SnO_2(IV). The initial discharge capacities of the

Li_2O-SnO_2-CuO-C, Li_2O-SnO_2-Cu_2O-C, and Li_2O-SnO_2-Cu-C nanocomposite powders were 1174, 1178, and 846 mAh g^{-1}, respectively. The reduction of CuO to metallic Cu ($CuO + 2Li^+ + 2e^-$ --> $Cu + Li_2O$) in the first discharge cycle did not occur in the Li_2O-SnO_2-Cu-C nanocomposite powder. Therefore, the powders treated at 500°C had lower initial discharge capacity than those of powders treated at temperatures below 450°C. The recombination of Cu and Li_2O occurred at an approximate voltage of 2.5 V in the Li_2O-SnO_2-CuO-C, and Li_2O-SnO_2-Cu_2O-C nanocomposite powders, as can be observed in the gently sloping curves in Fig. 4a above 2 V. The Cu metal formed from the first discharge cycle was available to react with Li_2O [28]. On the other hand, the recombination of Cu and Li_2O did not occur in the Li_2O-SnO_2-Cu-C nanocomposite powder during the first charge cycle because the crystalline Cu structure was too large to be electrochemically active, as shown by the XRD pattern of Li_2O-SnO_2-Cu-C in Fig. 3. The initial charge capacities of the Li_2O-SnO_2-CuO-C and Li_2O-SnO_2-Cu-C nanocomposite powders in voltage ranges above 2.0 V were 231 and 88 mAh g^{-1}, respectively. The Cu_6Sn_5-Cu_3Sn-C nanocomposite powder treated at a high temperature of 600°C had low initial discharge and charge capacities of 476 and 261 mAh g^{-1}, respectively. The initial irreversible capacity losses of the powders treated at 400, 450, 500, and 600°C were 333, 394, 299, and 215 mAh g^{-1}, respectively. The irreversible capacity losses of the composite powders in the first cycle were related to the formation/deformation of Li_2O as well as the solid electrolyte interface layer formation, irrespective of the post-treatment temperatures [29,30].

Cyclic voltammograms (CVs) as shown in Fig. 5 (b), (c), and (d) were generated at a scan rate of 0.1 mV s^{-1} during the first four cycles for electrodes produced using Li_2O-SnO_2-CuO-C, Li_2O-SnO_2-Cu_2O-C, and Li_2O-SnO_2-Cu-C nanocomposite powders. Reduction peaks at approximately 0.8 V in the CV profiles for the initial cycle clearly indicated that an irreversible reaction occurred during the initial discharge in all the samples. These reduction peaks disappeared in the CV profiles for the second cycle, and only the peaks at low potentials (<0.5 V), corresponding to Li-Sn alloy formation, were observed. The CV profiles of the Li_2O-SnO_2-CuO-C and Li_2O-SnO_2-Cu_2O-C nanocomposite powders had reduction peaks at approximately 1.3 V, which were related to the reduction of CuO or Cu_2O to Cu. The reduction peaks at 1.3 V were also observed in subsequent cycles. The Cu metal formed in the first discharge cycle was electrochemically available to react with Li_2O. Therefore, repeated reduction and oxidation of CuO occurred. The reduction peaks at approximately 1.3 V were not observed in the CV curves of the Li_2O-SnO_2-Cu-C nanocomposite powder. The Cu metal in this powder was electrochemically inactive because of the large crystallite size.

Fig. 6 (a) shows the cycling performance of the nanocomposite powders at a constant current density of 700 mA g^{-1}. The Li_2O-SnO_2-CuO-C and Li_2O-SnO_2-Cu_2O-C powders formed at post-treatment temperatures of 400 and 450°C, respectively, had poor cycling performances, while the Li_2O-SnO_2-Cu-C and Cu_6Sn_5-Cu_3Sn-C powders containing the highly conductive metal or alloys had superior cycling performances. The uniform mixing of electrochemically inactive Cu metal and electrochemically active SnO_2, as shown in the dot-mapping image of the powders in Fig. 1, improved the cycling performance of the Li_2O-SnO_2-Cu-C nanocomposite powder. The charge capacity dropped from 547 to 449 mAh g^{-1} after 130 cycles, and the corresponding capacity retention was 82%. The capacity retentions of the Li_2O-SnO_2-CuO-C and Li_2O-SnO_2-Cu_2O-C nanocomposite powders after

130 cycles were 44 and 52%, respectively. The charge capacity of the Cu_6Sn_5-Cu_3Sn-C nanocomposite powder after 130 cycles was 213 mAh g^{-1}.

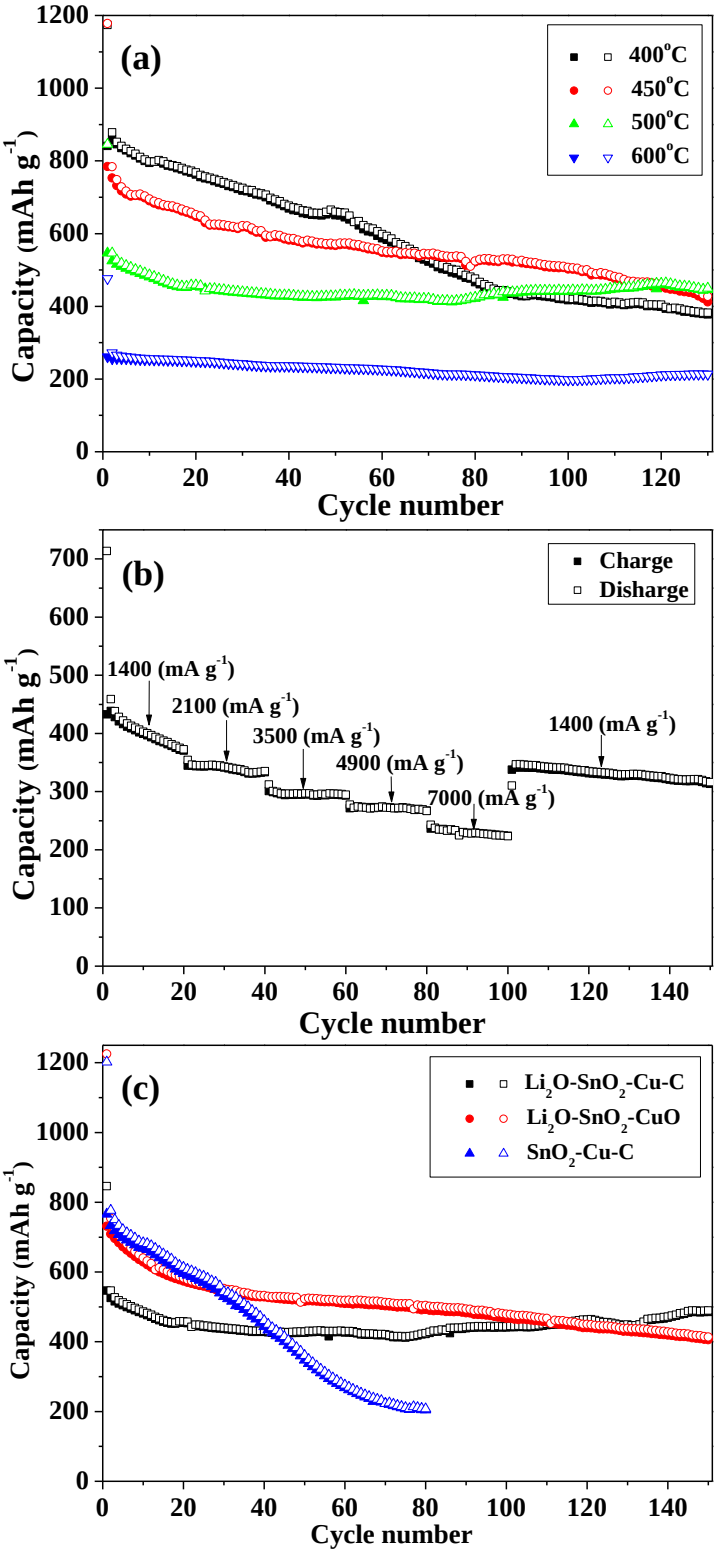

Figure 6. Cycle properties of the nanocomposite powders. (a) Cycle performances of Li_2O-SnO_2-Cu-C powder at 700 mA g^{-1}. (b) Rate performances of Li_2O-SnO_2-Cu-C powder. (c) Cycle performances of Li_2O-SnO_2-Cu-C, Li_2O-SnO_2-CuO and SnO_2-Cu-C.

The rate performance of the Li_2O-SnO_2-Cu-C nanocomposite powder as shown in Fig. 6 (b) was measured in the voltage range 0.01–3 V with a step-wise increase in current density from 1400 to 7000 mA g^{-1} before returning to 1400 mA g^{-1} The initial charge capacity of the powder was 432 mAh g^{-1} at a charge/discharge rate of 1400 mA g^{-1}. Even at a very high charge/discharge rate of 7000 mA g^{-1} and after 100 cycles, the charge capacity of this powder remained as high as 223 mAh g^{-1}. After 100 cycles, the charge capacity of the powder recovered significantly when the charge/discharge rate was returned to 1400 mA g^{-1}. The uniform mixing of highly conductive Cu metal and fine SnO_2 crystals improved the rate performance of Li_2O-SnO_2-Cu-C powder.

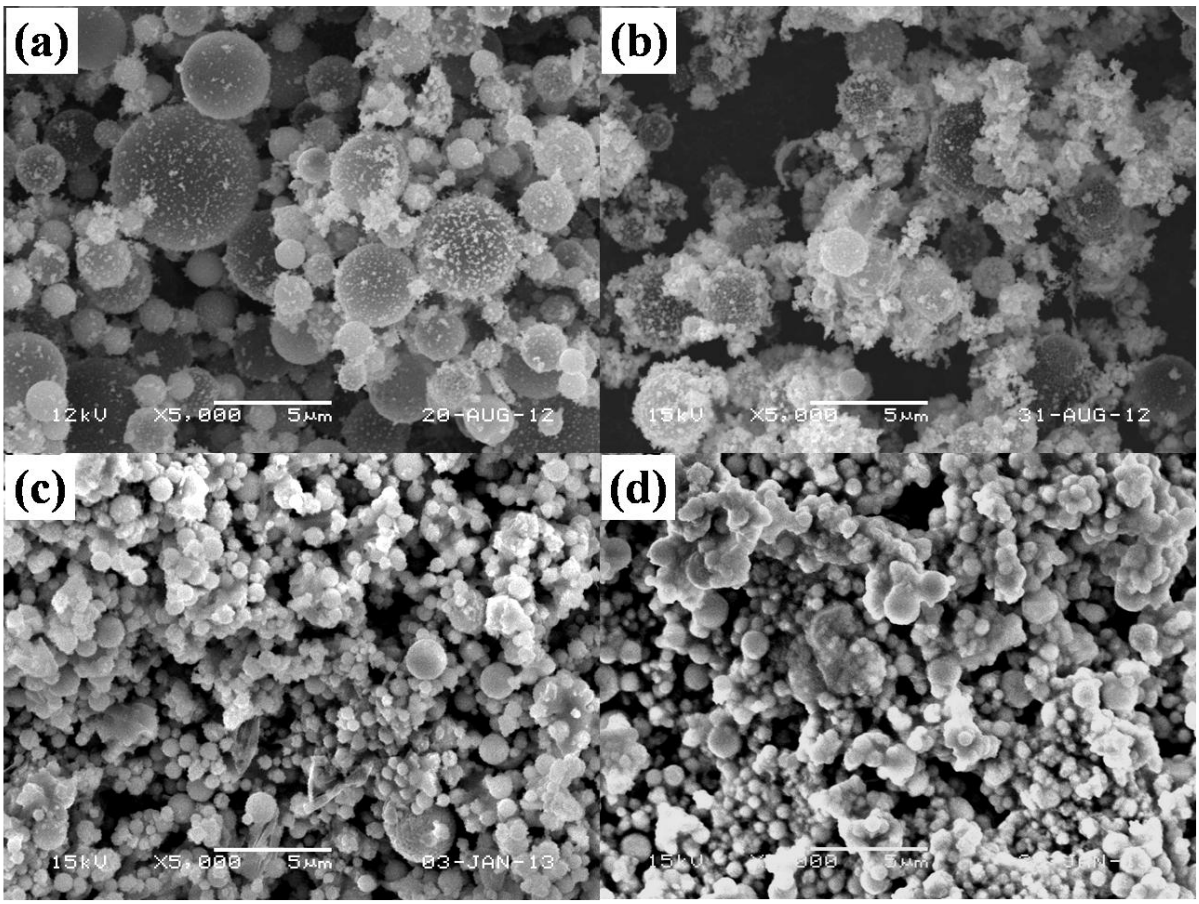

Figure 7. SEM images of the composite powders; (a) SnO_2-CuO-C, (b) SnO_2-Cu-C post-treated at 500°C, (c) Li_2O-SnO_2-CuO, (d) Li_2O-SnO_2-CuO post-treated at 500°C.

The effects of Li_2O and the C matrix on the cycle properties of the nanocomposite powders are shown in Fig. 6 (c). SnO_2-CuO-C and Li_2O-SnO_2-CuO nanocomposite powders were prepared directly by spray pyrolysis. The powders prepared by spray pyrolysis were post-treated at 500°C under a N_2 atmosphere. CuO in the SnO_2-CuO-C nanocomposite powder reduced to form SnO_2-Cu-C nanocomposite. In contrast, the reduction of CuO did not occur in the C-free Li_2O-SnO_2-CuO powder under the N_2 atmosphere. The morphologies of the nanocomposite powders before and after post-treatment were shown in Fig. 7. The morphology of the nanocomposite powders did not change after

post-treatment under pure N_2 atmosphere. The cycle properties of the SnO_2-Cu-C and Li_2O-SnO_2-CuO nanocomposite powders were compared to those of the Li_2O-SnO_2-Cu-C powder. The charge capacity of the SnO_2-Cu-C nanocomposite powder without Li_2O dropped from 766 to 204 mAh g^{-1} after 80 cycles, whereas the charge capacity of the C-free Li_2O-SnO_2-CuO nanocomposite powder dropped from 731 to 405 mAh g^{-1} after 150 cycles. Thus, Li_2O and the C matrix improved the rate and cycling performances of the Li_2O-SnO_2-Cu-C nanocomposite powder by minimizing the crystal growth of SnO_2 during repeated charging and discharging cycles.

4. CONCLUSIONS

The Li_2O-SnO_2-CuO-C nanocomposite powder was directly prepared by spray pyrolysis from an aqueous spray solution containing sucrose. The post-treatment of the prepared powders at 400, 450, 500, and 600°C under a N_2 atmosphere produced the Li_2O-SnO_2-CuO-C, Li_2O-SnO_2-Cu_2O-C, Li_2O-SnO_2-Cu-C, and Cu_6Sn_5-Cu_3Sn-C nanocomposite powders, respectively. The Cu metal formed in the first discharge cycle of the Li_2O-SnO_2-CuO-C and Li_2O-SnO_2-Cu_2O-C nanocomposite powders was electrochemically available to react with Li_2O. On the other hand, the Cu metal in the Li_2O-SnO_2-Cu-C nanocomposite powder was electrochemically inactive because of its large crystallite size. The Li_2O-SnO_2-Cu-C nanocomposite powder displayed desirable electrochemical performance, even at current densities above 700 mA g^{-1}. The presence of Li_2O and the C matrix improved the rate and cycling performances of the Li_2O-SnO_2-Cu-C nanocomposite powder by minimizing the crystal growth of SnO_2 during repeated charging and discharging cycles.

ACKNOWLEDGEMENT
This study was supported by the Converging Research Center Program through the National Research Foundation of Korea (NRF) funded by the Ministry of Education, Science and Technology (2011-50210).

References

1. F. Belliard, J.T.S. Irvine, *J. Power Sources*, 97 (2001) 219.
2. F. Chen, Z. Shi, M. Liu, *Chem. Commun*., 21 (2000) 2095.
3. D.W. Kim, I.S. Hwang, S.J. Kwon, H.Y. Kang, K.S. Park, Y.J. Choi, K.J. Choi, J.G. Park, *Nano Lett*., 7 (2007) 3041.
4. X.Y. Xue, B. He, S. Yuan, L.L. Xing, Z.H. Chen, C.H. Ma, *Nanotechnology*, 22 (2011) 395702.
5. C. Li, W. Wei, S.M. Fang, H.X. Wang, Y. Zhang, Y.H. Gui, R.F. Chen, *J. Power Sources*, 195 (2010) 2939.
6. M.F. Hassan, M.M. Rahman, Z.P. Guo, Z.X Chen, H.K. Liu, *J. Mater. Chem*., 20 (2010) 9707.
7. R.K. Selvan, N. Kalaiselvi, C.O. Augustin, C.H. Doh, C. Sanjeeviraja, *J. Power Sources*, 157 (2006) 522.
8. S.H. Choi, J.S. Kim, Y.S. Yoon, *Electrochim. Acta*, 50 (2004) 437.
9. T. Matsumura, N. Sonoyama, R. Kanno, M. Takano, *Solid State Ionics*, 158 (2003) 253.
10. Y. Liang, J. Fan, X.H. Xia, Y.S. Luo, Z.J. Jia, *Electrochim. Acta*, 52 (2007) 5891.
11. Y.Y. Wang, Y.J. Hao, Q.Y. Lai, J.Z. Lu, Y.D. Chen, X.Y. Ji, *Ionics*, 14 (2008) 85.

12. Y.M. Lin, R.K. Nagarale, K.C. Klavetter, A. Heller, C.B. Mullins, *J. Mater. Chem*., 22 (2012) 11134.
13. O. Mao, J.R. Dahn, *J. Electrochem. Soc*., 146 (1999) 423.
14. J. Hassoun, S. Panero, G. Mulas, B. Scrosati, *J. Power Sources*, 171 (2007) 928.
15. H. Guo, H. Zhao, X. Jia, *Electrochem. Commun*., 9 (2007) 2207.
16. Y. Yu, C.H. Chen, Y. Shi, *Adv. Mater*., 19 (2007) 993.
17. P. Zhang, Z.P. Guo, S.G. Kang, Y.J. Choi, C.J. Kim, K.W. Kim, H.K. Liu, *J. Power Sources*, 189 (2009) 566.
18. Y. Yu, C.H. Chen, J.L. Shui, S. Xie, *Angew. Chem. Int. Ed*., 117 (2005) 7247.
19. Y. Yu, Y. Shi, C.H. Chen, *Nanotechnology*, 18 (2007) 055706.
20. H.G. Jung, S.T. Myung, C.S. Yoon, S.B. Son, K.H. Oh, K. Amine, B. Scrosati, Y.K. Sun, *Energy Environ. Sci*., 4 (2011) 1345.
21. M.J. Noh, Y.J. Kwon, H.J. Lee, J.P. Cho, Y.J. Kim, M.G. Kim, *Chem. Mater*., 17 (2005) 1926.
22. N. Dimov, S. Kugino, M. Yoshio, *Electrochim. Acta*, 48 (2003) 1579.
23. W.M. Zhang, J.S. Hu, Y.G. Guo, S.F. Zheng, L.S. Zhong, W.G. Song, L.J. Wan, *Adv. Mater*., 20 (2008) 1160.
24. W.M. Zhang, X.L. Wu, J.S. Hu, Y.G. Guo, L.J. Wan, *Adv. Funct. Mater*., 18 (2008) 3941.
25. H. Wang, Q. Pan, J. Zhao, G. Yin, P. Zuo, *J. Power Sources*, 167 (2007) 206.
26. X.W. Lou, C.M. Li, L.A. Archer, *Adv. Mater*., 21 (2009) 2536.
27. J.Y. Xiang, J.P. Tu, Y.F. Yuan, X.L. Wang, X.H. Huang, Z.Y. Zeng, *Electrochim. Acta*, 54 (2009) 1160.
28. P. Poizot, S. Laruelle, S. Grugeon, L. Dupont, J.M. Tarascon, *Nature*, 407 (2000) 496.
29. M.G. Kim, S.J. Sim, J.P. Cho, *Adv. Mater*., 22 (2010) 5154.
30. C.Q. Zhang, J.P. Tu, X.H. Huang, Y.F. Yuan, X.T. Chen, F. Mao, *J. Alloys Compd*., 441 (2007) 52.

© 2013 by ESG (www.electrochemsci.org)